16 Quantifying Spatial Correlations in General Quantum Dynamics

Markus Müller
Peter-Grünberg-Institut 2
Forschungszentrum Jülich

Contents

E. Pavarini and E. Koch (eds.)
Topology, Entanglement, and Strong Correlations
Modeling and Simulation Vol. 10
Forschungszentrum Jülich, 2020, ISBN 978-3-95806-466-9
http://www.cond-mat.de/events/correl20

1 Introduction

Correlated dynamics play a key role in many aspects of our world, ranging from collective behavior of swarms of animals, correlations in the fluctuations of share prices at the stock market, to dynamical processes determining our weather. In physics, correlations in the dynamics of interacting many-body systems lie at the heart of our understanding of collective dynamical phenomena. Understanding the role of correlations in quantum systems is both a fundamental challenge and of high practical relevance for the control of multi-particle quantum systems, for example in the context of the ongoing efforts to build large-scale quantum computers and quantum simulators [1, 2]. Whereas most research has been focusing on various types of correlations that can be present in the *states* of quantum systems, in this lecture, our main focus will be on correlations that can be present in the *dynamics* of quantum systems. In particular, we will be discussing some basics of quantum dynamics in closed and open quantum systems, and introduce and discuss a general and rigorous method to quantify the amount of correlations in general dynamics of quantum systems. We will then apply these methods to various physical examples, such as the correlated decay of excited atoms coupled to the radiation field, and to the characterization of noise characteristics in real experimental trapped-ion quantum computers.

1.1 Temporal vs spatial correlations

Between what types of correlations in the dynamics of quantum systems can we distinguish? Quantum systems can display a wide variety of dynamical behaviors, in particular in open quantum systems, which are systems that are coupled to the surrounding environment. One interesting feature which has attracted much attention is the presence of memory effects (non-Markovianity) in the time evolution. Such *temporal* effects typically arise for strong enough coupling between the system and its environment, or when the environment is structured [3–5]. Whereas memory effects (or time correlations) can be present in any quantum system exposed to noise, another extremely relevant feature, which we will focus on in this lecture, are correlations in the dynamics of different parts of composite, i.e., multi-partite quantum systems. Since different parties of a partition are often, though not always, identified with different places in space, we will in the following refer to these correlations between subsystems of a larger quantum system as *spatial* correlations.

Spatial correlations in the dynamics give rise to a wide plethora of interesting phenomena, such as super-radiance [6] and decoherence-free subspaces [7–9], which we will also discuss as part of this lecture, and other phenomena like super-decoherence [10] and sub-radiance [11].

Moreover, clarifying the role of spatial correlations in the performance of a large variety of quantum processes is a highly active area of research, e.g. in quantum computing. There, spatially correlated noise can substantially reduce the parameter regimes and lower the error thresholds below which errors can be successfully fought off by quantum error correction techniques [12–14]. Other areas of interest are understanding the role of spatial correlations in the quantum dynamics underlying photosynthesis and excitation transfer [15, 16], and applications in quantum metrology [17].

As already mentioned, numerous works have aimed at quantifying up to which extent quantum dynamics deviates from the Markovian behavior. However, much less attention has been paid to developing quantifiers of spatial correlations in the dynamics. This may be partially due to the well-known fact that under many, though not all practical circumstances, dynamical correlations can be detected by studying the time evolution of correlation functions of properly chosen observables $\mathcal{O}_A$ and $\mathcal{O}_B$, acting respectively on the two parties A and B of a composite system S of interest. Indeed, any correlation $C(\mathcal{O}_A, \mathcal{O}_B) = \langle \mathcal{O}_A \otimes \mathcal{O}_B \rangle - \langle \mathcal{O}_A \rangle \langle \mathcal{O}_B \rangle$ detected during the time evolution of an initial product state, $\rho = \rho_A \otimes \rho_B$, witnesses the correlated character of the dynamics. Here, ρ_A and ρ_B denote the initial density operators of the two subsystems. However, it is a priori not easy to guess suitable observables. Furthermore there exist highly correlated dynamics, which cannot be realized by a combination of local processes and which do not generate any such correlation, e.g. a swap process between two parties.

Thus, it is important to develop methods which allow one to detect the presence or absence of spatial correlations in the dynamics, without a priori knowledge of the underlying microscopic dynamics, and which do not require one to resort to adequately chosen "test" observables and initial "test" quantum states. Such methods should furthermore provide a rigorous ground to quantitatively compare the amount of spatial correlations in different dynamical processes. These characteristics are essential for a "good" correlation quantifier that can be used to study spatial correlations in quantum dynamics from a fundamental point of view, to clarify their role in physical processes, as well as to measure and quantify spatial correlations in the dynamics of experimental quantum systems.

In this lecture, we will introduce first basic concepts of correlations in quantum states and quantum dynamics, and then introduce methods to quantify the degree of correlation in general quantum dynamics.

1.2 Correlations in quantum states

Before discussing quantum dynamics, let us, however, take a step back and first consider correlations that can be present in quantum states: a famous example of quantum-mechanically perfectly correlated states are Bell states [12], also called EPR-pairs, named after Einstein, Podolsky and Rosen [18]. An example is the following state of two qubits A and B

$$\left|\Phi^+\right\rangle_{\mathrm{AB}} = \frac{1}{\sqrt{2}}\Big(\left|0\right\rangle_{\mathrm{A}} \otimes \left|0\right\rangle_{\mathrm{B}} + \left|1\right\rangle_{\mathrm{A}} \otimes \left|1\right\rangle_{\mathrm{B}} \Big) = \frac{1}{\sqrt{2}}\Big(\left|00\right\rangle_{\mathrm{AB}} + \left|11\right\rangle_{\mathrm{AB}} \Big), \tag{1}$$

where $|0\rangle$ and $|1\rangle$ denote the computational basis states of each qubit (or spin-1/2 particle). Here and in the following we will mostly suppress the tensor-product symbol, for simplicity and compactness of notation. If now, say, the first qubit is measured in the computational basis, i.e., the state is projected onto either $|0\rangle_1$ or $|1\rangle_1$ (the eigenstates of the Pauli matrix $Z = |0\rangle\langle 0| - |1\rangle\langle 1|$), each of the two possible measurement outcomes $+1$ (for $|0\rangle_1$) and -1 (for $|1\rangle_1$) will be obtained with probability $1/2$. If the second qubit is also measured, it will be found with certainty in the same state as the first qubit – the measurement outcomes will be perfectly correlated. Note that this measurement statistics could also be explained by purely

classical correlations: think of a machine that with probability of 50% prepares both qubits in $|00\rangle_{\rm AB}$, and with 50% in $|11\rangle_{\rm AB}$ – the resulting measurement statistics would be the same. But what happens if the qubits of the Bell state (1) are measured in the X-basis instead, i.e., the observable Pauli matrix $X = |0\rangle\langle 1| + |1\rangle\langle 0|$ is measured? The Bell state can be equally written as

$$|\Phi^+\rangle_{\rm AB} = \frac{1}{\sqrt{2}}\Big(|00\rangle_{\rm AB} + |11\rangle_{\rm AB} \Big) = \frac{1}{\sqrt{2}}\Big(|{+}{+}\rangle_{\rm AB} + |{-}{-}\rangle_{\rm AB} \Big) \tag{2}$$

with $|\pm\rangle = \big(|0\rangle \pm |1\rangle \big)/\sqrt{2}$ denoting the eigenstates of X, $X|\pm\rangle = \pm|\pm\rangle$. Thus, the measurement outcomes for measurements in this different basis are also perfectly correlated! This feature is a signature of the entangled nature of this two-qubit state: in fact, there exists no basis, in which $|\Phi^+\rangle_{\rm AB}$ can be written as a product of single-qubit states $|\psi_1\rangle_{\rm A}$ and $|\psi_2\rangle_{\rm B}$, $|\Phi^+\rangle \neq |\psi_1\rangle_{\rm A} \otimes |\psi_2\rangle_{\rm B}$ – therefore, the two qubits are entangled.

How can one then quantify the amount of correlations in a bi-partite quantum state? This can be done by means of the quantum mutual information, which is a generalization of the Shannon mutual information in the classical case [12], which quantifies the mutual dependence between two random variables. Let us start by considering the density matrix $\rho_{\rm S}$ describing the joint state of a system S, which is composed of two parts A and B. The von Neumann entropy $S(\rho_{\rm S})$ of the state $\rho_{\rm S}$ is defined by

$$S(\rho_{\rm S}) := -{\rm Tr}\rho_{\rm S}\log(\rho_{\rm S}) \tag{3}$$

The density operator $\rho_{\rm S}$ can be written in terms of its eigenstates $|\psi_i\rangle$, $\rho_{\rm S} = \sum_i p_i |\psi_i\rangle\langle\psi_i|$, with $p_i \geq 0$ and $\sum_i p_i = 1$. Then the expression for the von Neumann entropy reduces to $S(\rho_{\rm S}) = -\sum_i p_i \log p_i$. For the system S in a pure state $|\psi\rangle$, $\rho_{\rm S} = |\psi\rangle\langle\psi|$, and $S(\rho_{\rm S}) = 0$.

The reduced density operators, associated to parts A and B of the composite system, $\rho_{\rm S}|_{\rm A}$ and $\rho_{\rm S}|_{\rm B}$, are obtained by performing the partial trace [12] over the respective complementary parts

$$\rho_{\rm S}|_{\rm A} = {\rm Tr}_{\rm B}(\rho_{\rm S}), \qquad \rho_{\rm S}|_{\rm B} = {\rm Tr}_{\rm A}(\rho_{\rm S}). \tag{4}$$

For the Bell state of Eq. (1), the reduced density operators correspond to the fully mixed state

$$\rho_{\rm S}|_{\rm A} = \frac{1}{2}\Big(|0\rangle\langle 0|_{\rm A} + |1\rangle\langle 1|_{\rm A} \Big), \qquad \rho_{\rm S}|_{\rm A} = \frac{1}{2}\Big(|0\rangle\langle 0|_{\rm B} + |1\rangle\langle 1|_{\rm B} \Big), \tag{5}$$

and thus the von Neumann entropies evaluate to $S(\rho_{\rm S}|_{\rm A}) = S(\rho_{\rm S}|_{\rm B}) = \log 2$.

Now, the quantum mutual information of a state $\rho_{\rm S}$ is given by

$$I(\rho_{\rm S}) = S(\rho_{\rm S}|_{\rm A}) + S(\rho_{\rm S}|_{\rm B}) - S(\rho_{\rm S}). \tag{6}$$

For the Bell state of Eq. (1) the quantum mutual information assumes its maximum value for a two-qubit system, $I(\rho_{\rm S}) = 2\log 2$, indicating that the Bell states are indeed *maximally correlated* quantum states. On the other hand, for any product state, i.e., if $\rho_{\rm S} = \rho_{\rm S}|_{\rm A} \otimes \rho_{\rm S}|_{\rm B}$, the quantum mutual information vanishes, which indicates that the subsystems A and B are independent. In order words, outcomes of local measurements on subsystems A and B are in the latter case *completely uncorrelated*, and thus from measuring one subsystem no information

about the state of the other subsystem can be inferred. Thus, quantum mutual information, as its classical counterpart, indicates by how much knowing about one part of a larger system reduces the uncertainty about the other part.

Finally, how can correlations in quantum states be detected in practice, i.e., in an experiment? As discussed, they reveal themselves in correlations in the measurement statistics of suitably chosen observables: Non-vanishing values for correlation functions such as $C(\mathcal{O}_\mathrm{A}, \mathcal{O}_\mathrm{B}) = \langle \mathcal{O}_\mathrm{A} \otimes \mathcal{O}_\mathrm{B} \rangle - \langle \mathcal{O}_\mathrm{A} \rangle \langle \mathcal{O}_\mathrm{B} \rangle$ signal the presence of correlations. For the example of the Bell state of Eq. (1), the choice of, e.g., $\mathcal{O}_\mathrm{A} = Z_\mathrm{A}$ and $\mathcal{O}_\mathrm{B} = Z_\mathrm{B}$ is suitable, since $\langle Z_\mathrm{A} \rangle = \mathrm{Tr}_\mathrm{A}(Z_\mathrm{A} \rho_\mathrm{S}|_\mathrm{A}) = 0$, and similarly for qubit B, whereas $\langle Z_\mathrm{A} \otimes Z_\mathrm{B} \rangle = +1$. In contrast, for a product state such as e.g. $|0\rangle_\mathrm{A} \otimes |0\rangle_\mathrm{B}$, the correlator expectation value vanishes, $C(Z_\mathrm{A}, Z_\mathrm{B}) = 0$.

2 Quantum dynamics

2.1 Closed- and open-system quantum dynamics

After this brief discussion about correlations that can be present in quantum *states*, let us turn our attention to quantum *dynamics*. General time evolution of a quantum system S, which can be coupled to an environment, can be described by quantum operations $\mathcal{E}_\mathrm{S}$ [3]. Here, we will focus on completely positive and trace-preserving (CPT) maps, often also called Kraus maps, which map valid physical density matrices describing the state of the system S onto other physical density matrices

$$\mathcal{E}_\mathrm{S} : \rho_\mathrm{S} \mapsto \mathcal{E}_\mathrm{S}(\rho_\mathrm{S}) = \sum_i K_i \, \rho_\mathrm{S} \, K_i^\dagger. \tag{7}$$

Here, the set of so-called Kraus operators $\{K_i\}$ fulfill $\sum_i K_i^\dagger K_i = \mathbb{1}_\mathrm{S}$. Note that this includes the case of time evolution in closed quantum systems, where $\rho_\mathrm{S} \mapsto U_\mathrm{S} \, \rho_\mathrm{S} \, U_\mathrm{S}^\dagger$, i.e., one Kraus operator corresponds to the unitary time evolution operator U_S and all other Kraus operators vanish.

As an example for open-system dynamics let us briefly discuss dephasing dynamics of a single qubit or spin-1/2 system. This dynamics is present in many physical systems, and it is a limiting factor in almost all architectures that are being used for quantum processors. Such dynamics can be generated for instance by fluctuating fields (e.g. magnetic background fields) in the lab. We can thus describe the dephasing process using a single fluctuating variable $B(t)$, referred to in the following as effective magnetic field

$$H_G(t) = \frac{1}{2} \, B(t) \, Z. \tag{8}$$

For simplicity, we assume the random fluctuation in the values of the effective magnetic field to obey a Gaussian distribution $P(B)$, which implies that

$$\left\langle \exp\left[\pm \mathrm{i} \int_0^t B(t')dt' \right] \right\rangle = \exp\left[-\frac{1}{2} \left\langle \left(\int_0^t B(t')dt' \right)^2 \right\rangle \right]. \tag{9}$$

If one additionally assumes a stationary autocorrelation function of the noise source

$$\big\langle B(t+\tau)\, B(t)\big\rangle = \big\langle B(\tau)\, B(0)\big\rangle, \tag{10}$$

and furthermore a δ-correlation of the noise, one obtains that

$$\big\langle B(\tau)\, B(0)\big\rangle = \big\langle [B(0)]^2\big\rangle\, \delta(\tau). \tag{11}$$

Using these properties, one finds

$$\left\langle \left[\int_0^t B(t')dt'\right]^2 \right\rangle = \big\langle [B(0)]^2\big\rangle t = \gamma t, \tag{12}$$

where we have defined the dephasing rate $\gamma = \big\langle [B(0)]^2\big\rangle$.
For an arbitrary initial (pure) state, $\rho(0) = |\psi(0)\rangle\langle\psi(0)|$, with $|\psi(0)\rangle = \alpha\,|0\rangle + \beta\,|1\rangle$, the state at time t will be given by an average over the noise realizations

$$\rho(t) = \int |\psi(t)\rangle\langle\psi(t)|\, P(B)\, dB = |\alpha|^2\,|0\rangle\langle 0| + |\beta|^2\,|1\rangle\langle 1| + e^{-\frac{1}{2}\gamma t}\big(\alpha\beta^*\,|0\rangle\langle 1| + \alpha^*\beta\,|1\rangle\langle 0|\big). \tag{13}$$

This allows us to identify this process as the dephasing channel [12]

$$\mathcal{E}_{\rm S} : \rho_{\rm S} \mapsto (1-p)\rho_{\rm S} + pZ\rho_{\rm S}Z, \tag{14}$$

i.e., as a quantum operation with the two Kraus operators $K_0 = \sqrt{1-p}\,\mathbb{1}$ and $K_1 = \sqrt{p}Z$ and the identification $p = \frac{1}{2}(1 - e^{-\frac{1}{2}\gamma t})$. Thus, for long times ($t \to \infty$, $p \to 1/2$), the initial coherence (off-diagonal elements of the density matrix (13)) completely vanishes and the qubit ends in an incoherent mixture of the computational basis states.

2.2 Detection of correlated dynamics

Let us now generalize our previous discussions in Sec. 1.2 about two qubits and consider a general bipartite quantum system $\mathrm{S} = \mathrm{AB}$ undergoing some dynamics given by a completely positive and trace preserving (CPT) map $\mathcal{E}_{\rm S}$. Without loss of generality we will assume that the dimension of both subsystems A and B is the same, $\dim(\mathcal{H}_{\rm A}) = \dim(\mathcal{H}_{\rm B}) = d$, and therefore $d_{\rm S} := \dim(\mathcal{H}_{\rm S}) = d^2$. The dynamics $\mathcal{E}_{\rm S}$ is said to be uncorrelated with respect to the subsystems A and B if it can be decomposed as $\mathcal{E}_{\rm S} = \mathcal{E}_{\rm A} \otimes \mathcal{E}_{\rm B}$, with individual CPT maps $\mathcal{E}_{\rm A}$ and $\mathcal{E}_{\rm B}$ acting on the subsystems A and B, respectively. Otherwise we call it correlated.
Simple examples of correlated dynamics from the field of quantum information are, e.g., two-qubit entangling gates, such as the prototypical two-qubit controlled-NOT (or CNOT) gate [12]

$$\text{CNOT} = |0\rangle\langle 0|_{\rm A} \otimes \mathbb{1}_{\rm B} + |1\rangle\langle 1|_{\rm A} \otimes X_{\rm B} \tag{15}$$

which flips the state of the target qubit (B), $|0\rangle \leftrightarrow |1\rangle$, if and only if the control qubit (A) is in the $|1\rangle$ state. For suitably chosen input product states, e.g. $|\psi(0)\rangle = |+\rangle_1 \otimes |0\rangle_2$, this unitary

gate creates (maximally) correlated output states such as the Bell state of Eq. (1), therefore the CNOT gate is clearly a correlated quantum dynamics!
Similarly, spatially homogeneous or *global* (magnetic) field fluctuations, acting with the same strength on a register of two or more qubits, described by a Hamiltonian

$$H_G(t) = \frac{1}{2} B(t) \sum_k Z_k \tag{16}$$

result in spatially correlated dephasing dynamics. This dynamics $\mathcal{E}_{\rm S}$ on the qubit register cannot be described by a product of independent dephasing processes, $\mathcal{E}_{\rm S} \neq \otimes_k \mathcal{E}_k$, with $\mathcal{E}_k$ acting on the k-th qubit. It is left as an exercise to work out the generalization of Eq. (14) for this scenario of correlated dephasing dynamics. Again, working with suitably chosen input states, e.g. $|\psi(0)\rangle = \otimes_k |+\rangle_k$, should allow one to distinguish between spatially correlated and uncorrelated dephasing.
In fact, this idea holds true in general: any correlation $C(\mathcal{O}_{\rm A}, \mathcal{O}_{\rm B}) = \langle \mathcal{O}_{\rm A} \otimes \mathcal{O}_{\rm B} \rangle - \langle \mathcal{O}_{\rm A} \rangle \langle \mathcal{O}_{\rm B} \rangle$ detected during the time evolution of an initial product state, $\rho_{\rm S} = \rho_{\rm A} \otimes \rho_{\rm B}$, witnesses the correlated character of the dynamics. However, for this to work, one needs to be lucky or have a priory knowledge about the dynamics and thereby be able to choose suitable observables and input states, for which correlated dynamics generates non-vanishing correlations in the final quantum state generated by the dynamics. Furthermore, note that there exist highly correlated dynamics, which cannot be realized by a combination of local processes, which however do not generate any such correlation. A simple example is the swap process between two parties. Such dynamics can either act on internal degrees of freedom, induced, e.g., by the action of a swap gate acting on two qubits [12], or can correspond to (unwanted) external dynamics, caused, e.g., by correlated hopping of atoms in an optical lattice [19] or the melting of an ion Coulomb crystal and subsequent recooling dynamics with a possibly different rearrangement of particles in trapped-ion architectures [20].

3 Rigorous quantifier for correlations in quantum dynamics

In light of this discussion, let us therefore now discuss a systematic and rigorous method to capture and quantify spatial correlations in quantum dynamics, not requiring any a-priori knowledge or assumptions about the dynamics taking place on the composite quantum system.

3.1 Choi-Jamiołkowski isomorphism

The central tool of our construction is the Choi-Jamiołkowski isomorphism [21, 22, 12]. This is a one-to-one correspondence of a given quantum dynamics of a system to an equivalent representation in the form of a quantum state in an enlarged Hilbert space. As we will see, this mapping will allow us to use tools developed for the quantification of correlations in quantum *states*, as we discussed above in Sec. 1.2, for our purpose of quantifying correlations in the quantum *dynamics* taking place in the bi-partite system ${\rm S} = {\rm AB}$. For this mapping, consider a

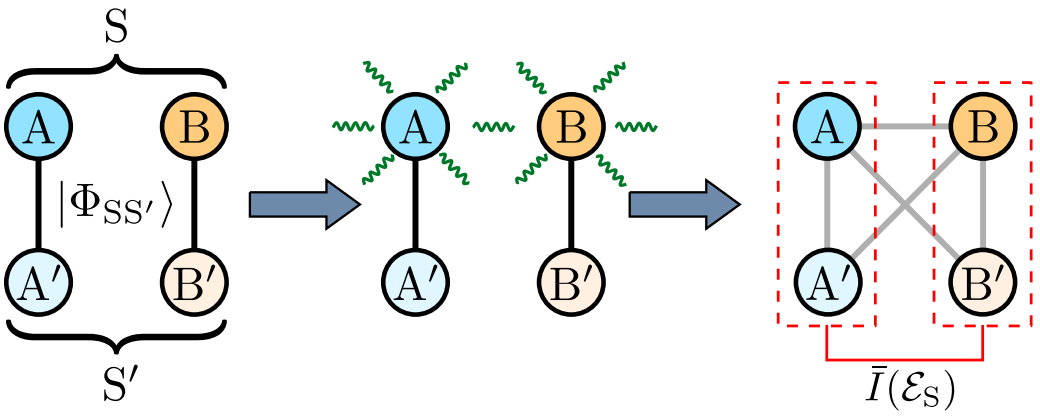

Fig. 1: *Schematics of the method. Left: the system S is prepared in a maximally entangled state* $|\Phi_{SS'}\rangle$ *with the auxiliary system* S′. *This state is just a product of maximally entangled states between* AA′ *and* BB′, *see Eq. (17). Middle: the system undergoes some dynamics* $\mathcal{E}_S$. *Right: if and only if this process is correlated with respect to* A *and* B, *the total system* SS′ *becomes correlated with respect to the bipartition* AA′|BB′. *The degree of correlation of the dynamics can then be measured by the normalized mutual information, see Eq. (20).*

second d^2-dimensional bipartite system $S' = A'B'$, essentially a "copy" of system S. Next, let $|\Phi_{SS'}\rangle$ be the maximally entangled state between S and S′,

$$|\Phi_{SS'}\rangle := \frac{1}{d}\sum_{j=1}^{d^2} |jj\rangle_{SS'} = \frac{1}{d}\sum_{k,\ell=1}^{d} |k\ell\rangle_{AB} \otimes |k\ell\rangle_{A'B'}\,. \tag{17}$$

Here, $|j\rangle$ denotes the state vector with 1 at the j-th position and zero elsewhere, i.e., the canonical basis in the d^2-dimensional Hilbert space of S and its "copy" S′. Similarly, $|k\rangle_A$ and $|l\rangle_B$ denote the canonical basis of the d-dimensional subsystems A, B, and A′, B′. The Choi-Jamiołkowki representation of some CPT map $\mathcal{E}_S$ on S is then given by the d^4-dimensional quantum state

$$\rho_S^{CJ} := \mathcal{E}_S \otimes \mathbb{1}_{S'}\big(\,|\Phi_{SS'}\rangle\langle\Phi_{SS'}|\,\big). \tag{18}$$

This means it is obtained by acting with the quantum operation $\mathcal{E}_S$ on S, and the identity operation $\mathbb{1}_{S'}$ on S′, as shown schematically in the middle part of Fig. 1. The entire information about the dynamical process $\mathcal{E}_S$ taking place in S is now contained in this unique state ρ_S^{CJ} in the enlarged d^4-dimensional space.

To become familiar with the Choi-Jamiołkowki representation of a quantum process, it is a useful exercise to show that for a system S consisting of a single qubit, which undergoes dephasing dynamics as described by Eq. (14), the Choi-Jamiołkowki state (18) reads

$$\rho_S^{CJ} = \frac{1}{2}\Big(\,|00\rangle\langle 00|_{SS'} + |11\rangle\langle 11|_{SS'}\,\Big) + \frac{1}{2}(1-2p)\Big(\,|00\rangle\langle 11|_{SS'} + |11\rangle\langle 00|_{SS'}\,\Big). \tag{19}$$

3.2 Construction of a correlation measure

In order to formulate a faithful measure of spatial correlations for dynamics, we adopt a resource theoretic approach (see, e.g., [23, 24] where this approach is used in the context of entanglement theory). The idea is that one may consider correlated dynamics as a resource to perform whatever task that cannot be implemented solely by (composing) uncorrelated evolutions $\mathcal{E}_{\mathrm{A}} \otimes \mathcal{E}_{\mathrm{B}}$. Then, suppose that the system S undergoes some dynamics given by the map $\mathcal{E}_{\mathrm{S}}$. Now, consider the (left and right) composition of $\mathcal{E}_{\mathrm{S}}$ with some uncorrelated maps $\mathcal{L}_{\mathrm{A}} \otimes \mathcal{L}_{\mathrm{B}}$ and $\mathcal{R}_{\mathrm{A}} \otimes \mathcal{R}_{\mathrm{B}}$, which act before and after $\mathcal{E}_{\mathrm{S}}$, so that the total dynamics is given by $\mathcal{E}'_{\mathrm{S}} = (\mathcal{L}_{\mathrm{A}} \otimes \mathcal{L}_{\mathrm{B}})\mathcal{E}_{\mathrm{S}}(\mathcal{R}_{\mathrm{A}} \otimes \mathcal{R}_{\mathrm{B}})$. It is clear that any task that we can do with $\mathcal{E}'_{\mathrm{S}}$ by composition with uncorrelated maps can also be achieved with $\mathcal{E}_{\mathrm{S}}$ by composition with uncorrelated maps. Hence, we assert that the amount of correlation in $\mathcal{E}_{\mathrm{S}}$ is at least as large as in $\mathcal{E}'_{\mathrm{S}}$. In other words, the amount of correlations of some dynamics does not increase under composition with uncorrelated dynamics. This is the fundamental law of this resource theory of spatial correlations for dynamics, and any faithful measure of correlations should satisfy it. For the sake of comparison, in the resource theory of entanglement, entanglement is the resource, and the fundamental law is that entanglement cannot increase under application of local operations and classical communication (LOCC) [23]. For example, the entangled state of Eq. (1) can be transformed via the local unitary X_B on qubit B into another Bell state $\frac{1}{\sqrt{2}}(|01\rangle_{\mathrm{AB}} + |10\rangle_{\mathrm{AB}})$, with the same amount of entanglement. However, a product state of two qubits, not having any entanglement, cannot be transformed into an entangled state by local operations such as single-qubit gate operations or local measurements on A and B, or classical communication between the two single-qubit subsystems A and B. In this spirit, we introduce a measure of correlations for dynamics [25] via the (normalized) quantum mutual information of the Choi-Jamiołkowski state $\rho_{\mathrm{S}}^{\mathrm{CJ}}$, Eq. (18),

$$\bar{I}(\mathcal{E}_{\mathrm{S}}) := \frac{I(\rho_{\mathrm{S}}^{\mathrm{CJ}})}{4\log d} := \frac{1}{4\log d}\Big(S\left(\rho_{\mathrm{S}}^{\mathrm{CJ}}|_{\mathrm{AA}'}\right) + S\left(\rho_{\mathrm{S}}^{\mathrm{CJ}}|_{\mathrm{BB}'}\right) - S\left(\rho_{\mathrm{S}}^{\mathrm{CJ}}\right)\Big). \tag{20}$$

Here, $S(\cdot) := -\mathrm{Tr}[(\cdot)\log(\cdot)]$ is again the von Neumann entropy, now evaluated for the reduced density operators $\rho_{\mathrm{S}}^{\mathrm{CJ}}|_{\mathrm{AA}'} := \mathrm{Tr}_{\mathrm{BB}'}(\rho_{\mathrm{S}}^{\mathrm{CJ}})$ and $\rho_{\mathrm{S}}^{\mathrm{CJ}}|_{\mathrm{BB}'} := \mathrm{Tr}_{\mathrm{AA}'}(\rho_{\mathrm{S}}^{\mathrm{CJ}})$; see Fig. 1. In essence, here we apply the quantum mutual information and von Neumann entropy we have seen in Sec. 1.2 for quantum states, now to the Choi-Jamiołkowski state, which is equivalent to the quantum dynamics taking place on system S.

But why is the quantity $\bar{I}(\mathcal{E}_{\mathrm{S}})$ a good and faithful measure of how correlated the dynamics given by $\mathcal{E}_{\mathrm{S}}$ is? The reason is that it satisfies the following desired properties:

i) The quantity $\bar{I}(\mathcal{E}_{\mathrm{S}}) = 0$ if and only if $\mathcal{E}_{\mathrm{S}}$ corresponds to uncorrelated dynamics, $\mathcal{E}_{\mathrm{S}} = \mathcal{E}_{\mathrm{A}} \otimes \mathcal{E}_{\mathrm{B}}$. This follows from the fact that the Choi-Jamiołkowski state of an uncorrelated map is a product state with respect to the bipartition $\mathrm{AA}'|\mathrm{BB}'$ (no proof given here).

ii) The quantity $\bar{I}(\mathcal{E}_{\mathrm{S}}) \in [0, 1]$. It is clear that $\bar{I}(\mathcal{E}_{\mathrm{S}}) \geq 0$, moreover it reaches its maximum value when $S(\rho_{\mathrm{S}}^{\mathrm{CJ}})$ is minimal and $S\left(\rho_{\mathrm{S}}^{\mathrm{CJ}}|_{\mathrm{AA}'}\right) + S\left(\rho_{\mathrm{S}}^{\mathrm{CJ}}|_{\mathrm{BB}'}\right)$ is maximal. Both conditions are met when $\rho_{\mathrm{S}}^{\mathrm{CJ}}$ is a maximally entangled state with respect to the bipartition $\mathrm{AA}'|\mathrm{BB}'$, leading to $I(\rho_{\mathrm{S}}^{\mathrm{CJ}}) = 2\log d^2$.

iii) The fundamental law of the resource theory for correlations in quantum dynamics is satisfied, namely that

$$\bar{I}(\mathcal{E}_{\mathrm{S}}) \geq \bar{I}\big((\mathcal{L}_{\mathrm{A}} \otimes \mathcal{L}_{\mathrm{B}})\mathcal{E}_{\mathrm{S}}(\mathcal{R}_{\mathrm{A}} \otimes \mathcal{R}_{\mathrm{B}})\big), \tag{21}$$

stating that the amount of correlations of the dynamics $\mathcal{E}_{\mathrm{S}}$ decreases or at most stays the same, if the dynamics is composed with uncorrelated dynamics. Stated differently, if a process is a composition of a correlated and an uncorrelated part, the amount of correlations in the composition has to be equal or smaller than the amount of correlation that is inherent to the correlated part. Here, equality in the above inequality is reached for composition with uncorrelated unitary dynamics, $\mathcal{L}_{\mathrm{A}}(\cdot) = U_{\mathrm{A}}(\cdot)U_{\mathrm{A}}^{\dagger}$, $\mathcal{L}_{\mathrm{B}}(\cdot) = U_{\mathrm{B}}(\cdot)U_{\mathrm{B}}^{\dagger}$, $\mathcal{R}_{\mathrm{A}}(\cdot) = V_{\mathrm{A}}(\cdot)V_{\mathrm{A}}^{\dagger}$, and $\mathcal{R}_{\mathrm{B}}(\cdot) = V_{\mathrm{B}}(\cdot)V_{\mathrm{B}}^{\dagger}$.

Leaving aside the normalization factor $1/(4\log d)$, the quantifier (20) can be intuitively understood as the amount of information that is needed to distinguish the actual dynamics $\mathcal{E}_{\mathrm{S}}$ from the individual dynamics of its parts $\mathcal{E}_{\mathrm{S}_1} \otimes \mathcal{E}_{\mathrm{S}_2}$ [12]. Namely, the information that is lost when $\mathcal{E}_{\mathrm{S}_1} \otimes \mathcal{E}_{\mathrm{S}_2}$ is taken as an approximation of $\mathcal{E}_{\mathrm{S}}$. The normalized quantity $\bar{I} \in [0,1]$ quantifies this information relative to the maximum value it can take on all possible processes.
For clarity, we remark that the use of an ancilla system S' is merely underlying the mathematical construction of the isomorphism. It is not required in an experimental determination of $\bar{I}$. Rather than reconstructing the Choi-Jamiołkowski state $\rho_{\mathrm{S}}^{\mathrm{CJ}}$ from quantum state tomography [12] on the enlarged system SS', one can equivalently determine $\rho_{\mathrm{S}}^{\mathrm{CJ}}$ by reconstructing the dynamics $\mathcal{E}_{\mathrm{S}}$ by means of quantum process tomography on the physical system S alone. For a system S of N qubits, due to the Choi-Jamiołkowski isomorphism the number of real parameters to determine, $4^N(4^N-1)$, is in both cases the same and grows exponentially with the number of qubits.

3.3 Maximally correlated quantum dynamics

Before computing $\bar{I}$ for some cases of physical interest it is worth studying which dynamics achieve the maximum value $\bar{I}_{\max} = 1$. From the resource theory point of view, these dynamics can be considered as maximally correlated since they cannot be constructed from other maps by composition with uncorrelated maps [because of Eq. (21)]. One can show the following property of maximally correlated dynamics:

Theorem 1. If for a map $\mathcal{E}_{\mathrm{S}}$ the property that $\bar{I}(\mathcal{E}_{\mathrm{S}}) = 1$ holds, it must be unitary $\mathcal{E}_{\mathrm{S}}(\cdot) = U_{\mathrm{S}}(\cdot)U_{\mathrm{S}}^{\dagger}$, $U_{\mathrm{S}}U_{\mathrm{S}}^{\dagger} = \mathbb{1}$.

Proof. As aforementioned, the maximum value, $\bar{I}(\mathcal{E}_{\mathrm{S}}) = 1$, is reached if and only if $\rho_{\mathrm{S}}^{\mathrm{CJ}}$ is a maximally entangled state with respect to the bipartition $\mathrm{AA}'|\mathrm{BB}'$, $|\Psi_{(\mathrm{AA}')|(\mathrm{BB}')}\rangle$. Then

$$\mathcal{E}_{\mathrm{S}} \otimes \mathbb{1}_{\mathrm{S}'}\big(\,|\Phi_{\mathrm{SS}'}\rangle\langle\Phi_{\mathrm{SS}'}|\,\big) = |\Psi_{(\mathrm{AA}')|(\mathrm{BB}')}\rangle\langle\Psi_{(\mathrm{AA}')|(\mathrm{BB}')}| \tag{22}$$

is a pure state. Therefore $\mathcal{E}_{\mathrm{S}}$ must be unitary as the Choi-Jamiołkowski state is pure if and only if it represents a unitary map. □

What are examples of maximally correlated dynamics? One example for such dynamics is the swap operation, exchanging the states of the two parties A and B, $U_{\mathrm{S}} = U_{\mathrm{A}\leftrightarrow\mathrm{B}}$, and thus also any unitary of the form of $(U_{\mathrm{A}} \otimes U_{\mathrm{B}})U_{\mathrm{A}\leftrightarrow\mathrm{B}}(V_{\mathrm{A}} \otimes V_{\mathrm{B}})$.

However, not every U_{S} that is maximally correlated falls into this class. For example, the unitary operation of two qubits $U'_{\mathrm{S}} = |21\rangle\langle 12| + \mathrm{i}\big(|11\rangle\langle 21| + |12\rangle\langle 11| + |22\rangle\langle 22|\big)$ is maximally correlated, however, it cannot be written as $(U_{\mathrm{A}} \otimes U_{\mathrm{B}})U_{\mathrm{A}\leftrightarrow\mathrm{B}}(V_{\mathrm{A}} \otimes V_{\mathrm{B}})$, since that would imply vanishing $\bar{I}(U'_{\mathrm{S}}U_{\mathrm{A}\leftrightarrow\mathrm{B}})$ whereas $\bar{I}(U'_{\mathrm{S}}U_{\mathrm{A}\leftrightarrow\mathrm{B}}) = 1/2 \neq 0$.

What about, e.g., the 2-qubit controlled-NOT (CNOT) gate? Interestingly, operations able to create highly correlated states such as the CNOT gate achieve a correlation value of 1/2 and thus do not correspond to maximally correlated dynamics. Note that whereas a CNOT gate creates, for appropriately chosen two-qubit initial states, maximally entangled states, there are other states which are left completely uncorrelated under its action. The measure $\bar{I}$ captures, completely independently of initial states and of whether possibly created correlations are quantum or classical, the fact that correlated dynamics cannot be realized by purely local dynamics.

This leads to the following question: Among the quantum processes of a given system which correspond to maximally correlated dynamics, is there one from which any other dynamics can be obtained – something like the mother of all dynamics?

In some resource theories, such as bipartite entanglement, this is the case: there the maximal element (e.g. a Bell state in a 2-qubit system) can generate any other element by applying the operations which fulfill its fundamental law, e.g. LOCC. This is not the case here, i.e., maximally correlated evolutions cannot generate any arbitrary dynamics by composition with uncorrelated operations. Indeed, if $\mathcal{E}_{\mathrm{S}}^{\max}$ were able to generate any other dynamics it would, in particular, be able to generate any unitary evolution U_{S}, $(\mathcal{L}_{\mathrm{A}} \otimes \mathcal{L}_{\mathrm{B}})\mathcal{E}_{\mathrm{S}}^{\max}(\mathcal{R}_{\mathrm{A}} \otimes \mathcal{R}_{\mathrm{B}})(\cdot) = U_{\mathrm{S}}(\cdot)U_{\mathrm{S}}^{\dagger}$. However, this would imply that $\mathcal{L}_{\mathrm{A}} \otimes \mathcal{L}_{\mathrm{B}}$, $\mathcal{E}_{\mathrm{S}}^{\max}$ and $(\mathcal{R}_{\mathrm{A}} \otimes \mathcal{R}_{\mathrm{B}})$ are unitary evolutions as well, so that $(U_{\mathrm{A}} \otimes U_{\mathrm{B}})U_{\mathrm{S}}^{\max}(V_{\mathrm{A}} \otimes V_{\mathrm{B}}) = U_{\mathrm{S}}$, with $\mathcal{E}_{\mathrm{S}}^{\max}(\cdot) = U_{\mathrm{S}}^{\max}(\cdot)U_{\mathrm{S}}^{\max\dagger}$. Since $\bar{I}(\mathcal{E}_{\mathrm{S}})$ is invariant under the composition of uncorrelated unitaries, this result would imply that for any correlated unitary U_{S}, $\bar{I}(U_{\mathrm{S}})$ would take the same value, $\bar{I}(U_{\mathrm{S}}^{\max})$, and this is not true, as we have seen for the examples of the swap operation and the CNOT gate.

4 Quantifying dynamical correlations in physical systems

4.1 Correlated dynamics of atoms in the electromagnetic vacuum

Let us now illustrate the behavior of $\bar{I}(\mathcal{E}_{\mathrm{S}})$ for the paradigmatic example of two identical two-level atoms interacting with the vacuum of the electromagnetic radiation field.

The free Hamiltonian of the atoms of transition frequency ω is

$$H_{\mathrm{S}} = \frac{\omega}{2}\big(Z_1 + Z_2\big) \tag{23}$$

with Z_j the Pauli-matrix for the j-th atom. In addition, the environmental free Hamiltonian

corresponds to the modes of the radiation field and is given by

$$H_{\rm E} = \sum_{\boldsymbol{k}} \sum_{\lambda=1,2} \omega_{\boldsymbol{k}} a^\dagger_\lambda(\boldsymbol{k}) a_\lambda(\boldsymbol{k}), \tag{24}$$

where $\boldsymbol{k}$ and λ stand for the wave vector and the two polarization degrees of freedom, respectively. We have taken natural units $\hbar = c = 1$. The dispersion relation in free space is $\omega_{\rm k} = |\boldsymbol{k}|$, and the field operators $a^\dagger_\lambda(\boldsymbol{k})$ and $a_\lambda(\boldsymbol{k})$ describe the creation and annihilation of photons with wave vector $\boldsymbol{k}$ and polarization vector $\boldsymbol{e}_\lambda$. These fulfill $\boldsymbol{k}\cdot\boldsymbol{e}_\lambda = 0$ and $\boldsymbol{e}_\lambda \cdot \boldsymbol{e}_{\lambda'} = \delta_{\lambda,\lambda'}$.
The atom-field interaction is described in dipole approximation by the Hamiltonian

$$H_{\rm SE} = -\sum_{j=1,2} \left[\sigma_j^- \boldsymbol{d}\cdot\boldsymbol{E}(\boldsymbol{r}_j) + \sigma_j^+ \boldsymbol{d}^*\cdot\boldsymbol{E}(\boldsymbol{r}_j)\right]. \tag{25}$$

Here, $\boldsymbol{d}$ is the dipole matrix element of the atomic transition, $\boldsymbol{r}_j$ denotes the position of the j-th atom, and the raising and lowering operators σ_j^+ and σ_j^- are defined as $\sigma_j^+ = (\sigma_j^-)^\dagger = |e\rangle_j\,{}_j\langle g|$ for its exited $|e\rangle_j$ and ground $|g\rangle_j$ states. Furthermore, the electric field operator is given (in Gaussian units)

$$\boldsymbol{E}(\boldsymbol{r}) = {\rm i}\sum_{\boldsymbol{k},\lambda} \sqrt{\frac{2\pi\omega_{\boldsymbol{k}}}{\mathcal{V}}}\boldsymbol{e}_\lambda(\boldsymbol{k})\left(a_\lambda(\boldsymbol{k}){\rm e}^{{\rm i}\boldsymbol{k}\cdot\boldsymbol{r}} - a^\dagger_\lambda(\boldsymbol{k}){\rm e}^{-{\rm i}\boldsymbol{k}\cdot\boldsymbol{r}}\right), \tag{26}$$

where $\mathcal{V}$ denotes the quantization volume. Under a series of standard assumptions known as the Markovian weak-coupling limit [3] the dynamics of the atoms is governed by a Lindblad master equation of the form

$$\frac{d\rho_{\rm S}}{dt} = \mathcal{L}(\rho_{\rm S}) = -{\rm i}\tfrac{\omega}{2}\big(Z_1 + Z_2, \rho_{\rm S}\big) + \sum_{i,j=1,2} a_{jk}\Big(\sigma_k^-\rho_{\rm S}\sigma_j^+ - \tfrac{1}{2}\{\sigma_j^+\sigma_k^-, \rho_{\rm S}\}\Big). \tag{27}$$

After taking the continuum limit ($\frac{1}{\mathcal{V}}\sum_{\boldsymbol{k}} \to \frac{1}{(2\pi)^3}\int d^3\boldsymbol{k}$) and performing the integrals, the coefficients a_{jk} are given by (see e.g. Sec. 3.7.5 of Ref. [3])

$$a_{jk} = \gamma_0\big(j_0(x_{jk}) + P_2(\cos\theta_{jk}) j_2(x_{jk})\big). \tag{28}$$

Here, $\gamma_0 = \frac{4}{3}\omega^3|\boldsymbol{d}|^2$, and $j_0(x)$ and $j_2(x)$ are spherical Bessel functions [26]

$$j_0(x) = \frac{\sin x}{x}, \quad j_2(x) = \left(\frac{3}{x^3} - \frac{1}{x}\right)\sin x - \frac{3}{x^2}\cos x, \tag{29}$$

and

$$P_2(\cos\theta) = \frac{1}{2}\big(3\cos^2\theta - 1\big) \tag{30}$$

is a Legendre polynomial, with

$$x_{jk} = \omega|\boldsymbol{r}_j - \boldsymbol{r}_k| \quad \text{and } \cos^2(\theta_{jk}) = \frac{|\boldsymbol{d}\cdot(\boldsymbol{r}_j - \boldsymbol{r}_k)|^2}{|\boldsymbol{d}|^2|\boldsymbol{r}_j - \boldsymbol{r}_k|^2}. \tag{31}$$

Notice that if the distance between atoms $r = |\boldsymbol{r}_1 - \boldsymbol{r}_2|$, is much larger than the wavelength associated with the atomic transition $r \gg 1/\omega$, we have $a_{jk} \simeq \gamma_0\delta_{ij}$ and only the diagonal

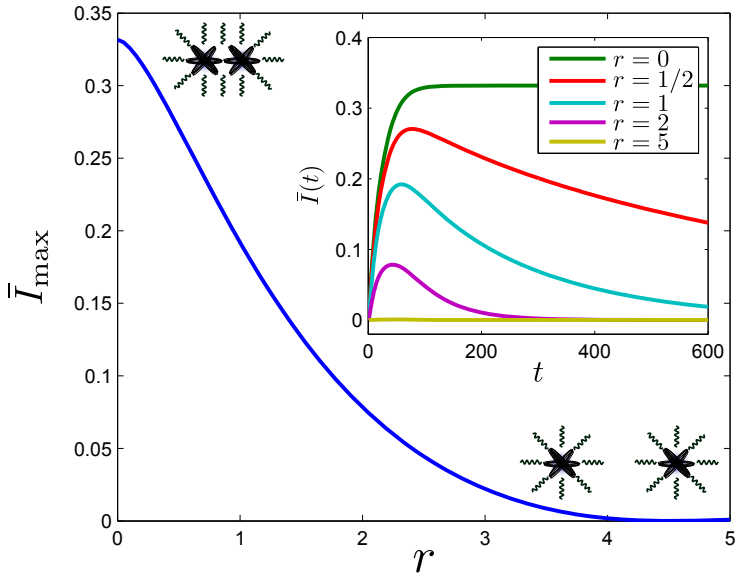

Fig. 2: *Maximum value of $\bar{I}$ as a function of the distance r for two two-level atoms radiating in the electromagnetic vacuum. As expected, the amount of correlations in the dynamics decreases with r. In the inset, $\bar{I}$ is represented as a function of time for different distances r between atoms ($\omega = |\boldsymbol{d}|/2 = 1$, θ=0). With increasing time, correlations in the dynamics build up, which for longer times decay to zero, except for the limit vanishing distance $r \to 0$ between the two atoms.*

terms $\gamma_0 = \frac{4}{3}\omega^3|\boldsymbol{d}|^2$ are relevant. Then, the master equation describes two-level atoms interacting with independent environments, and there are no correlations in the emission of photons by the first and the second atom. In the opposite case, when $r \ll 1/\omega$, every matrix element approaches the same value $a_{ij} \simeq \gamma_0$, in the master equation the atomic transitions can be approximately described by the collective jump operators $J_\pm = \sigma_1^\pm + \sigma_2^\pm$, and the pair of atoms becomes equivalent to a four-level system with Hamiltonian $\omega J_z = \frac{\omega}{2}(Z_1 + Z_2)$ at the mean position $(\boldsymbol{r}_1 - \boldsymbol{r}_2)/2$ interacting with the electromagnetic vacuum. This emission of photons in a collective way is known as super-radiance. It can be effectively described in terms of collective angular momentum operators and was first studied in the 1950s by Robert H. Dicke [6].

To quantitatively assess this behavior of uncorrelated/correlated dynamics as a function of the interatomic distance r, we can numerically compute the measure of correlations $\bar{I}$ according to Eq. (20). To this end, we consider a maximally entangled state $|\Phi_{\mathrm{SS}'}\rangle$ between two sets S and S′ of two qubits according to the maximally correlated state as given for the general case in Eq. (17). Namely, here S is the set of the two physical qubits, i.e., the two two-level atoms 1 and 2, and the "copy" system S′ is made up of two auxiliary qubits $1'$ and $2'$ as sketched in Fig. 1. Next, the part S of the maximally entangled state $|\Phi_{\mathrm{SS}'}\rangle\langle\Phi_{\mathrm{SS}'}|$ is evolved according to the master equation (27) while keeping the part S′ constant, to obtain $\rho_{\mathrm{S}}^{\mathrm{CJ}}(t)$. This can be done, for instance, by numerically integrating the master equation $\frac{d\rho_{\mathrm{S}}^{\mathrm{CJ}}(t)}{dt} = \mathcal{L} \otimes \mathbb{1}[\rho_{\mathrm{S}}^{\mathrm{CJ}}(t)]$, with the initial condition $\rho_{\mathrm{S}}^{\mathrm{CJ}}(0) = |\Psi_{\mathrm{SS}'}\rangle\langle\Psi_{\mathrm{SS}'}|$, where $\mathcal{L}$ is for the present example specified in Eq. (27). Tracing out qubits 2 and $2'$ of $\rho_{\mathrm{S}}^{\mathrm{CJ}}(t)$ yields $\rho_{\mathrm{S}}^{\mathrm{CJ}}(t)|_{11'}$, and similarly tracing out qubits 1 and $1'$ yields $\rho_{\mathrm{S}}^{\mathrm{CJ}}(t)|_{22'}$. Finally, this allows one to compute the von Neumann entropies of $\rho_{\mathrm{S}}^{\mathrm{CJ}}(t)|_{11'}$, $\rho_{\mathrm{S}}^{\mathrm{CJ}}(t)|_{22'}$ and $\rho_{\mathrm{S}}^{\mathrm{CJ}}(t)$ to calculate $\bar{I}(t)$ according to Eq. (20).

The results are shown in Fig. 2. Despite the fact that the value of $\bar{I}$ depends on time (the dynamical map is formally given by $\mathcal{E}_{\mathrm{S}} = \mathrm{e}^{t\mathcal{L}}$), the correlation quantifier $\bar{I}$ decreases as r increases, as expected. Furthermore, the value of $\bar{I}$ approaches zero for long times t (see inset plot), except in the limiting case of vanishing distance $r = 0$ between the two atoms. This is because for $r \neq 0$ the dynamics becomes uncorrelated in the asymptotic limit, $\lim_{t\to\infty} \mathrm{e}^{t\mathcal{L}} = \mathcal{E} \otimes \mathcal{E}$. Here, the single-qubit Kraus maps describing the dynamics of the composite two-atom system are given by $\mathcal{E}(\cdot) = K_1(\cdot)K_1^\dagger + K_2(\cdot)K_2^\dagger$ with Kraus operators $K_1 = \left(\begin{smallmatrix} 0 & 0 \\ 1 & 0 \end{smallmatrix}\right)$ and $K_2 = \left(\begin{smallmatrix} 0 & 0 \\ 0 & 1 \end{smallmatrix}\right)$. It can be checked from the form of this map that therefore for long times both atoms will eventually end up in the product state formed of both atoms in the ground state $|g\rangle$. However, for $r = 0$, $\lim_{t\to\infty} \mathrm{e}^{t\mathcal{L}}$ is a correlated map. Thus, we obtain perfect agreement between the rigorous measure of correlations $\bar{I}$ and the physically expected behavior of two distant atoms undergoing independent decay.

4.2 Noise characterization of an experimental quantum computer

In the following, we will apply the correlation quantifier to a second physical scenario. We will use it to study the dynamics of spatial correlations of noise processes that are present in a trapped ion quantum computer, which has been built by our collaborators in the experimental ion-trap group at Innsbruck, Austria [27], and for which we quantitatively characterized its spatial noise correlations in a recent joint project [28]. To date, trapped ions are one of most advanced platforms for quantum information processing, and a highly promising platform to build reliable and scalable quantum computers. Figure 3 shows the schematic of a linear-ion trap quantum processor.

Let us briefly describe the experimental platform used to implement the correlation characterization protocol. Each qubit is encoded in the $4S_{1/2}$ and $3D_{5/2}$ electronic states of a single $^{40}\mathrm{Ca}^+$ ion of a string of ions trapped in a macroscopic linear Paul trap [27]. Doppler cooling of the ion crystal is performed on a short-lived cycling transition between the $4S_{1/2}$ and the $4P_{1/2}$ levels, as illustrated in Fig. 4. The same transition is used to detect the qubit state via the electron shelving scheme. Two additional repumping lasers ensure that the ion does not get trapped in a dark state and enable resetting from the long-lived $3D_{5/2}$ state. A more detailed description of the tool-set and the experimental setup used can be found in [27].

To manipulate the state of the qubit, two different laser beams are used: A global beam effectively illuminates all ions in the chain with equal power and allows rotations of all qubits simultaneously. Therefore interactions of the following form are possible:

$$R_\phi(\theta) = \exp\left(-i\frac{\theta}{2}S_\phi\right), \tag{32}$$

where $S_\phi = \sum_{k=0}^{N}(X_k \cos\phi + Y_k \sin\phi)$ with X_k and Y_k being single-qubit Pauli matrices acting on qubit k.

To perform local operations on single qubits an addressed beam is available. This tightly focused beam is steered along the linear ion chain via an electro-optical deflector. By driving the

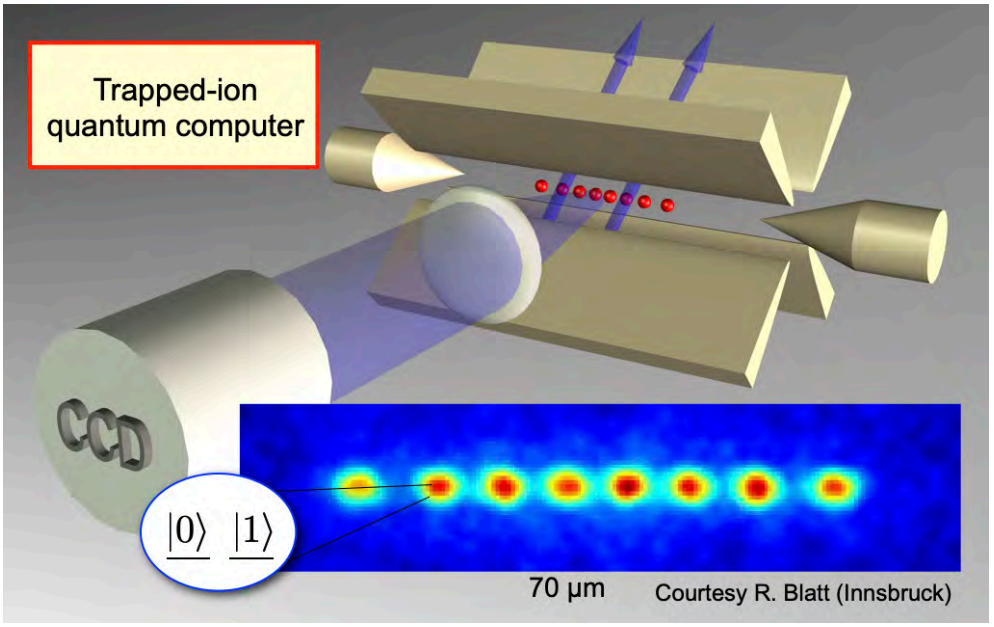

Fig. 3: *Schematics of a linear-ion-trap quantum computer. A linear Paul trap formed of metallic blades and endcap electrodes (at the left and right end of the trap) is used to apply a combination of static electric and oscillating radio-frequency fields, to create a confining potential in all three directions for the charged ions. Ions can be laser-cooled so that they form at sufficiently low temperatures self-assembled Coulomb crystals, such as shown in the fluorescence picture of a linear ion crystal. Here, the ion positions are determined by the interplay of mutual Coulomb repulsion between the ions and external confinement through the trapping fields. A pair of (meta-)stable electronic states is used to encode one qubit in each of the ions. Tightly focused as well as collectively applied laser beams are then be applied to the ions. These can be used to initialize the register of qubits to a well-defined initial state at the beginning of a quantum computation, to apply single-qubit gate operations and to read out the final state at the end of a quantum algorithm by collecting the light from state-dependent fluorescence imaging via a CCD camera. Two- or multi-qubit entangling gate operations can be implemented by coupling the electronic dynamics to the collective vibrational modes (phonons) of the ion crystal, which can thereby act as a quantum bus.*

qubit transition on resonance or in a detuned way, two types of rotations can be realized:

$$R_{\phi}^{(k)}(\theta) = \exp\left(-i\frac{\theta}{2}(X_k\cos\phi + Y_k\sin\phi)\right)$$

and

$$S_z^{(k)}(\theta) = \exp\left(-i\frac{\theta}{2}Z_k\right).$$

This control toolset allows one to prepare the qubits in the required initial state, encode them in different Zeeman sublevels and perform quantum process tomography. Entangling gates belong also to the gate set of the quantum processor [27], but are not needed for the noise correlation characterization protocol and therefore not discussed here.

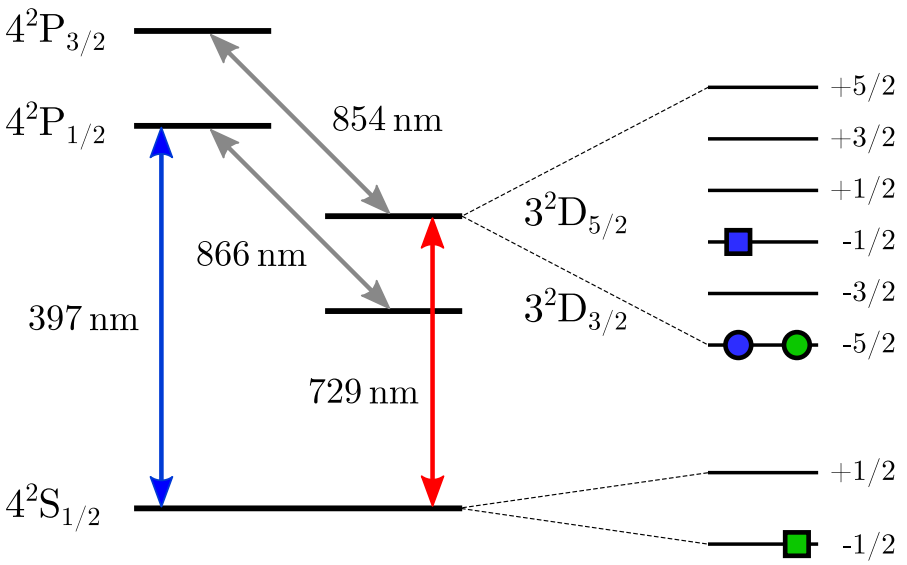

Fig. 4: *Electronic level scheme of $^{40}Ca^+$. The green and blue squares and circles indicate different qubit encodings, denoted **A** and **B**, respectively. Squares are marking the qubit state $|1\rangle$ whereas the state $|0\rangle$ is highlighted with circles. The corresponding frequency shifts of the transitions caused by the magnetic field are -2.80 MHz/G and $+3.36$ MHz/G for the qubits marked with green and blue symbols respectively. For configuration 1 described in the enumeration in the main text for both qubits the encoding marked in green is used. The asymmetry in scenario 2 is introduced by encoding one of the qubits in the states illustrated in blue. For the third configuration both qubits again use the encoding marked in green and the spontaneous decay from $|0\rangle$ to $|1\rangle$ is enhanced. Figure from [28].*

Let us now discuss how the temporal development of the spatial correlation estimator $\bar{I}$ can be used to determine the degree of spatial correlations in a two-qubit register. For this, we perform full quantum process tomography on qubit registers with varying degree of correlations. The electronic hyperfine level structure of the $^{40}Ca^+$ (see Fig. 4) is rich enough to allow the experimentalists to choose and investigate the noise characteristics for qubits encoded in various pairs of computational basis states. Here, the idea is that the degree of noise correlations between individual qubits can be tuned by encoding them in Zeeman states with differing magnetic field susceptibility. As a consequence, different sensitivities to noise from magnetic field fluctuations is expected. Concretely, there exist multiple possibilities to encode a qubit in the Zeeman levels of the $4S_{1/2}$ and $3D_{5/2}$ states as shown in Fig. 4. The susceptibility of the qubits to the magnetic field ranges from -2.80 MHz/G to $+3.36$ MHz/G, which allows the experimentalists to tune not only the coherence time of the individual qubits but also the *correlations* between qubits, when magnetic field fluctuations are the dominant source of noise.

Understanding the dephasing dynamics, and in particular noise correlations, in registers containing qubits in different encodings is essential in the context of error mitigation and quantum error correction: this understanding will be needed to determine the viability of an approach to build, e.g., functional logical qubits formed of entangled ensembles of physical qubits, which can be used to fight errors by means of quantum error correction techniques.

4.3 Experimental determination of spatial dynamical correlations

In the following we will consider dephasing dynamics that is caused by a magnetic field acting on a string of two ions. The various qubit-states have different susceptibilities to magnetic field fluctuations, given by the Landé g factors g_i of the involved Zeeman substates. The phase that qubit i accumulates during the time evolution is therefore given by

$$\phi_i(t) = \int_0^t d\tau B(\tau)\mu_b g_i$$

with the time-dependent magnitude of the magnetic field $B(\tau)$ and the Bohr magneton μ_b. The magnetic field fluctuations can be modeled by multiple random implementations of $B(t)$. The time evolution for a single implementation can then be expressed as

$$U(\phi_1) = \exp\left(-i\phi_1(\sigma_1^z + g\sigma_2^z)\right) \tag{33}$$

with the ratio of the Landé factors $g{=}g_2/g_1$. In order to estimate the dynamics under a dephasing decay, one needs to average the evolution over many noise realizations with random phases.
In the experiment we investigated the following qubit configurations that implement dephasing and spontaneous decay dynamics:

1. **Configuration 1:** For the realization of maximally correlated dephasing dynamics, both qubits are encoded in the $\left|4S_{1/2},\, m_S{=}{-}1/2\right\rangle$ and $\left|3D_{5/2},\, m_S{=}{-}5/2\right\rangle$ states. This encoding is referred to as encoding **A** hereinafter, and corresponds to the green markers in Fig. 4. Both qubits have a susceptibility to the magnetic field of -2.80 MHz/G, leading to identical susceptibility coefficients ($g = 1$) (see Eq. (33)).

2. **Configuration 2:** To introduce an asymmetric dephasing dynamics, one qubit is encoded in **A** and the second is encoded in the states $\left|3D_{1/2},\, m_S{=}{-}1/2\right\rangle$ and $\left|3D_{5/2},\, m_S{=}{-}5/2\right\rangle$ respectively. This encoding is referred to as encoding **B** hereinafter, and corresponds to the blue markers in Fig. 4. Their different susceptibilities to magnetic field noise of -2.80 MHz/G and $+3.36$ MHz/G introduce unequal dephasing and therefore are expected to affect correlations between the qubits, corresponding to the susceptibility coefficients ($g = -0.83$).

3. **Configuration 3:** Uncorrelated dynamics can be engineered in this experimental system by introducing spontaneous decay. In this scenario, both qubits are encoded in Encoding **A**. A laser pulse resonant with the $3D_{5/2} \leftrightarrow 4P_{3/2}$ transition at 854 nm shortens the effective lifetime of the exited state by inducing a spontaneous decay to the $4S_{1/2}, m_S = -1/2$ level via the short-lived $3P_{3/2}, m_S = -3/2$ level. Since spontaneous emission of visible photons by the ions at a distance of several micrometers corresponds to an uncorrelated noise process, as we have seen in Sec. 3, this controllable pump process implements an uncorrelated noise process that can be modeled as spontaneous decay. The effective lifetime depends on the laser power and is in our case set to be $T_{\text{spont}} = 7(1)\,\mu$s.

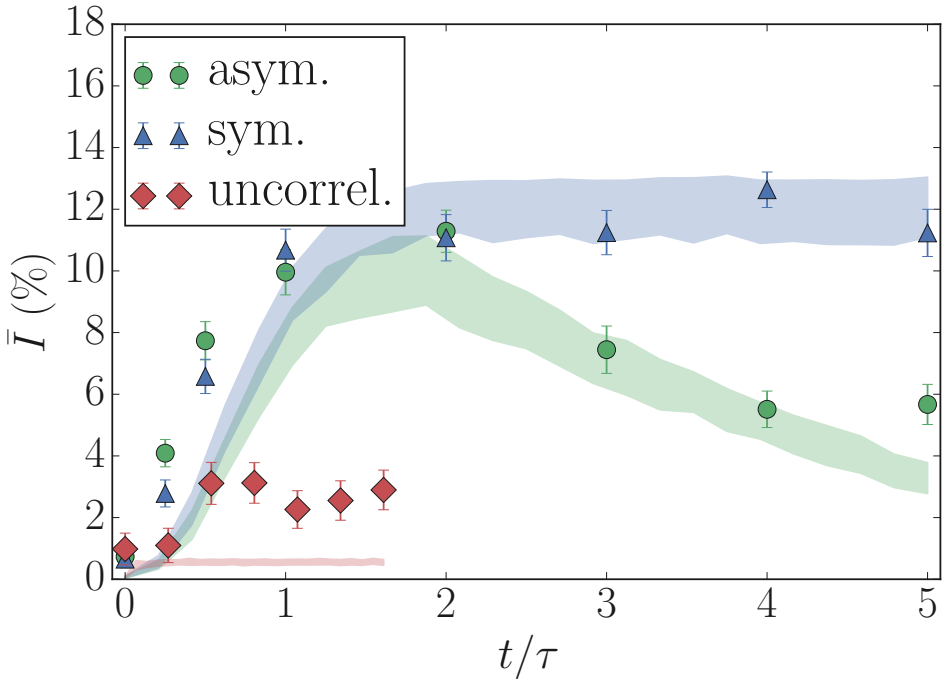

Fig. 5: *Dynamics of the spatial correlation quantifier $\bar{I}$ for different qubit encodings. Three cases are depicted: Both qubits encoded in $|4S_{1/2}, m_S{=}-1/2\rangle \leftrightarrow |3D_{5/2}, m_S{=}-5/2\rangle$ (blue triangles), one qubit encoded in $|4S_{1/2}, m_S{=}-1/2\rangle \leftrightarrow |3D_{5/2}, m_S{=}-5/2\rangle$ and $|3D_{1/2}, m_S{=}-1/2\rangle \leftrightarrow |3D_{5/2}, m_S{=}-5/2\rangle$ (green circles) and both qubits subject to uncorrelated dynamics via spontaneous decay (red diamonds). The horizontal axis is normalized to the coherence time for the first two cases and to the decay time for the third case. Results from a Monte Carlo based numerical simulations with 500 samples are depicted with shaded areas in the corresponding color. Figure from [28].*

The small quantum register consisting of only two qubits allows one to perform full process tomography [12] to fully reconstruct the dynamics $\mathcal{E}_{\mathrm{S}}$ in the two-qubit system. From this, the correlation measure $\bar{I}$ (see Eq. (20)) can be directly determined. In the present platform, the amplitude of the magnetic field fluctuations is non-stationary as it depends on the entire laboratory environment, e.g., due to fluctuating currents flowing through wires, which therefore cannot be controlled accurately. However, the apparatus allows one to engineer a stationary magnetic field noise as the dominating noise source (a situation where laser and magnetic field noise have to be taken into account is described in [28]). Thus we could control and tune the single qubit coherence time. The stationary magnetic field noise is engineered by our experimental colleagues by applying a white-noise current to the coils that generate the magnetic field at the ions' positions. The noise amplitude is set such that the coherence time of the qubit encoded in $\left|4S_{1/2}, m_S{=}-1/2\right\rangle$ and $\left|3D_{5/2}, m_S{=}-5/2\right\rangle$ is reduced from $59(3)$ ms to $1.98(7)$ ms. The increase of magnetic field noise by a factor of ≈ 30 ensures that laser phase-noise is negligible on these timescales. From the measured data, a process matrix fully describing $\mathcal{E}_{\mathrm{S}}$ was reconstructed using an iterative maximum likelihood method to ensure trace preservation and positivity of the process matrix.

The results for the estimated quantifier for spatial correlations as defined in Eq. (20) $\bar{I}$ are shown in Fig. 5 for the decoherence processes of the different configurations described above. These processes are described by an exponential decay and show different timescales. To compare the data from the different configurations we express the free evolution time in units of the respective decay times τ. The temporal development of $\bar{I}$ is studied for evolution times of up to 5 times the decoherence time for configurations 1 and 2 and up to 1.6 times the lifetime for configuration 3, as the differences in the dynamics of different correlation strength are most pronounced on those timescales.

It can be seen in Fig. 5 that **the symmetric configuration** (Configuration 1), depicted with blue triangles and labeled with *"sym."*, shows the highest degree of correlations that reaches a steady state for long evolution times. The correlations converge to a saturation value of 11.2(8) %, which is in agreement with the theoretical value of 12.5 % (as expected in the limit of perfectly correlated dephasing) within 2 standard deviations. It is left and suggested as an exercise to determine this value of $\bar{I} = 1/8$ for the case of perfectly correlated two-qubit dephasing dynamics, as we discussed above in Sec. 2.2 and described by the fluctuating field Hamiltonian Eq. (16).

Measurements using **the asymmetric configuration** (Configuration 2), depicted with green circles and labeled with *"asym."*, show similar dynamics to the symmetric setting for times up to twice the coherence time. For longer evolution times, however, a significant decrease in correlations is observed.

The third investigated scenario (Configuration 3) implementing engineered **uncorrelated** dynamics by adding spontaneous decay, is depicted with red diamonds. The correlations do not exceed a value of 3.1(6) % in this case. This is significantly lower than the maximum of $\bar{I}$ for fully and partially correlated dephasing dynamics.

The blue shaded area in the figure shows simulated results where random phase fluctuations are acting on a two-qubit system. Whereas there is qualitative agreement between simulations and measurements, there are still statistically significant deviations, especially in the case of uncorrelated dynamics, of up to approximately $4\,\sigma$. We assume that this overestimation of the spatial correlations in the system dynamics by the quantifier is due to mis-calibration and drifts of experimental parameters. For instance a mismatch between the actual and the calibrated Rabi frequency would lead to additional correlated errors during the process tomography. This effect is most pronounced for Configuration 3, where the dynamics are expected to show no correlations at all.

4.4 Decoherence-free subspaces and entanglement-based magnetometry

What can one learn from the build-up of strong correlations in the dynamics of qubits, as observed in particular for the symmetric encoding in Fig. 5 in the previous section? And can one use this information for useful applications? Can these correlations be harnessed to protect fragile qubit states from decoherence caused by correlated dephasing dynamics? The answer is yes!

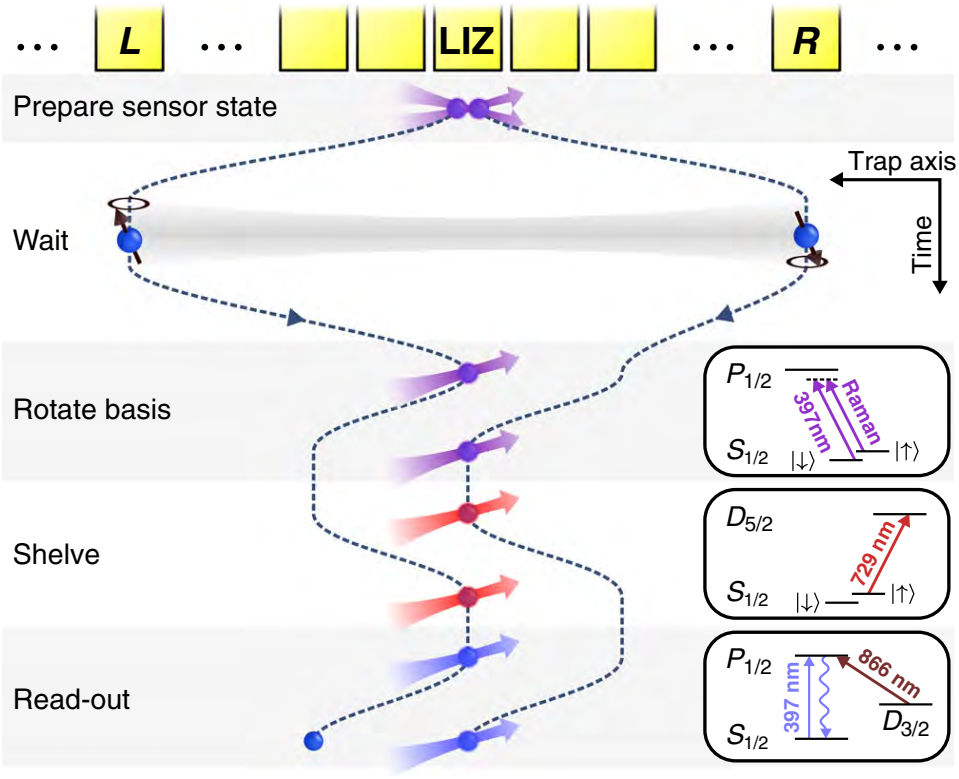

Fig. 6: *Experimental procedure implemented in [29] for measurements of inhomogenous magnetic fields in a segmented ion trap. After the creation of the sensor Bell state by means of single- and two-qubit gates in the laser interaction zone (LIZ), the two constituent ions are separated and shuttled to the desired trap segments L and R. In order to measure the accumulated phase during the interrogation time T, the ions are individually shuttled back to the LIZ to perform basis rotations that allow for state read-out via electron shelving and fluorescence detection in either the X_1X_2 or Y_1Y_2 measurement basis. For basis rotations, electron shelving, and fluorescence detection, the relevant energy levels are shown in the small inset figures at the right. Figure reproduced from [29].*

The key idea of how this works can be understood by considering a fluctuating magnetic field which acts with exactly the same magnitude, and thus *perfectly spatially correlated* on all qubits, as discussed above and described by Hamiltonian of Eq. (16). A single-qubit superposition state $|\psi\rangle_k = \alpha\,|0\rangle_k + \beta\,|1\rangle_k$ will under such noise dephase over time and end up in a classical mixture $|\rho\rangle_k = |\alpha|^2\,|0\rangle\langle 0|_k + |\beta|^2\,|1\rangle\langle 1|_k$. If we, however, consider instead a Bell state of two qubits,

$$|\psi\rangle_{12} = \alpha\,|01\rangle_{12} + \beta\,|10\rangle_{12}\,, \tag{34}$$

we find that under the time evolution generated by the collective dephasing Hamiltonian Eq. (16) such a superposition remains an eigenstate of the time evolution operator at all times. Or in other words, no relative phase in the superposition state (34) is accumulated. Therefore, under this correlated dephasing noise, the basis states $|01\rangle_{12}$ and $|10\rangle_{12}$ span a two-dimensional so-called decoherence-free subspace (DFS): this is a subspace of the two-qubit Hilbert space, within

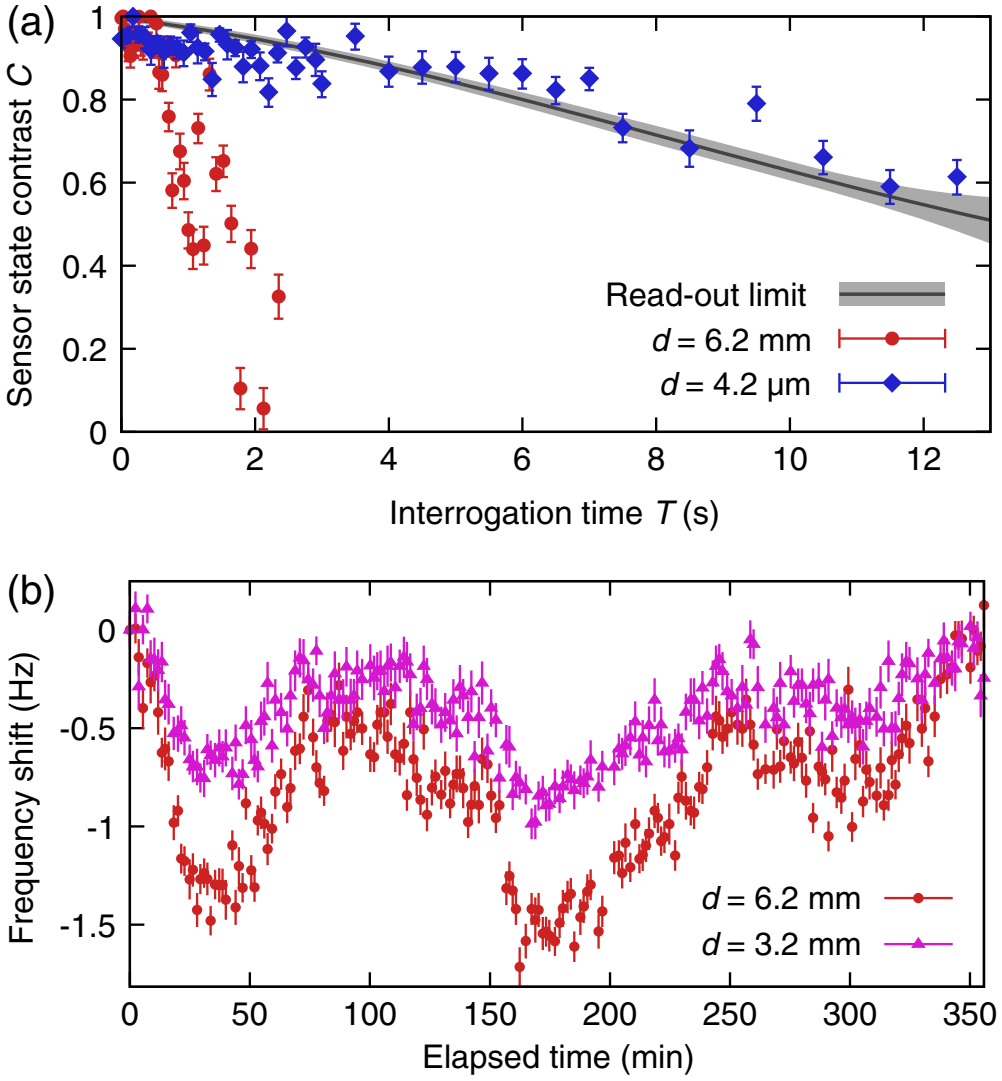

Fig. 7: *(a) Sensor state contrast C as a function of the interrogation time during which the two ions of the sensor Bell state (34) are exposed to the magnetic fields at their respective positions, spatially separated by a distance of $d = 6.2$ mm (red dots) and $d = 4.2$ µm (blue squares). For illustration, the black curve and gray region indicate a third-order polynomial fit to a separate read-out fidelity measurement and its confidence bands (see [29]). (b) Simultaneous drift of the measured frequency difference for ion distances $d = 6.2$ mm (blue circles) and $d = 3.2$ mm (purple triangles) over a duration of about 6 hours with an interrogation time of $T = 150$ ms. Figure reproduced from [29].*

which the noise acts trivially and quantum information can be stored and protected for longer times than in single physical qubits. Alternatively, one can view the state of Eq. (34) as a minimal "logical qubit" formed of two physical qubits, with effective logical basis states $|0\rangle_L = |01\rangle_{12}$ and $|1\rangle_L = |10\rangle_{12}$, and which offers protection against spatially correlated dephasing noise. Using such two-qubit DFS spaces in two ions, quantum information and entanglement can be preserved for timescales of minutes, as impressively demonstrated already in 2005 [9],

and which is to be contrasted to typical single-qubit coherence times of (tens) of milliseconds. What happens if the dephasing noise is spatially correlated, however, these correlations are not perfect? Can this be exploited as a measurement tool? In Ref. [29] it was shown that under these circumstances Bell states of the form (34) can be used as highly sensitive probe states to detect small spatially inhomogeneous dc magnetic fields. As discussed above, common-mode magnetic-field fluctuations are not seen by the entangled sensor state. In contrast, inhomogeneous components of the field can be detected! This gives rise to excellent sensitivity to small differences in local magnetic fields in different areas of the trap, separated by distances as large as 0.61mm. For comparison typical inter-ion distances in an ion Coulomb crystal are a few micrometer. The experimental setup and field gradient probing protocol is summarized in Fig. 6. Figure 7 shows experimental results of this technique, which allows to probe magnetic field differences over distances of several mm, and with spatial resolution as small as about 20 nm, and with accuracies down to 300 fT and sensitivities down to 12 pT/$\sqrt{\mathrm{Hz}}$.

5 Lower bounds, multi-partite systems, and outlook

The exact determination of the correlation quantifier $\bar{I}$ requires as input the process $\mathcal{E}_{\mathrm{S}}$, which can be reconstructed from quantum process tomography [12]. For small systems formed of only two qubits, this is feasible, it becomes, however, impractical for larger systems due to the exponential number of measurements required. The good news is that a lower estimate for $\bar{I}$ can be obtained by performing correlation measurements on the subsystems S_1 and S_2. Here, the central result is that the normalized quantity $\bar{I}(\mathcal{E}_{\mathrm{S}})$ is bounded from below by

$$\bar{I}(\mathcal{E}_{\mathrm{S}}) \geq \frac{1}{8\ln d}\frac{C^2_{\rho'}(\mathcal{O}_1,\mathcal{O}_2)}{\|\mathcal{O}_1\|^2\|\mathcal{O}_2\|^2}, \tag{35}$$

with two local quantum observables $\mathcal{O}_1$ and $\mathcal{O}_2$ and $C_{\rho'}(\mathcal{O}_1,\mathcal{O}_2) = \langle \mathcal{O}_1\otimes\mathcal{O}_2\rangle_{\rho'} - \langle\mathcal{O}_1\rangle_{\rho'}\langle\mathcal{O}_2\rangle_{\rho'}$. Here, $\rho' = \mathcal{E}_{\mathrm{S}}(\rho)$ is the evolution of an initial product state ρ according to the dynamical map $\mathcal{E}_{\mathrm{S}}$, while $\|\cdot\|$ denotes the operator norm (the absolute value of the maximum eigenvalue) and we have taken the logarithms inside $\bar{I}(\mathcal{E}_{\mathrm{S}})$ in Eq. (20) to be binary logarithms $\log_2$ (otherwise the natural logarithm $\ln d$ on the right hand side becomes multiplied by a different factor).

So far, we have focused our discussion on the characterization of correlations in the dynamics of bipartite quantum systems. The approach to measure and estimate bipartite correlations can be extended to the multi-partite case. In this situation, one has to specify what kind of correlations are the matter of interest. For instance, one may be interested in the amount of correlations shared between two parties of the system or between all parties. Figure 8 illustrates a generic situation where correlations among all systems are investigated. For example, suppose we consider the total amount of correlations, i.e., the amount of correlations shared by all parties. In that case, if the system S has M parties $\mathrm{S}_1,\mathrm{S}_2,\ldots,\mathrm{S}_M$, we can introduce respective ancillary systems $\mathrm{S}'_1,\mathrm{S}'_2,\ldots,\mathrm{S}'_M$ as we did in the bipartite case, and prepare a collection of M maximally entangled states between S_1 and S'_1, S_2 and S'_2, etc. [see Fig. 8(A)]. The dynamics is then applied on the system S we want to study. The amount of total (normalized) correlations in the

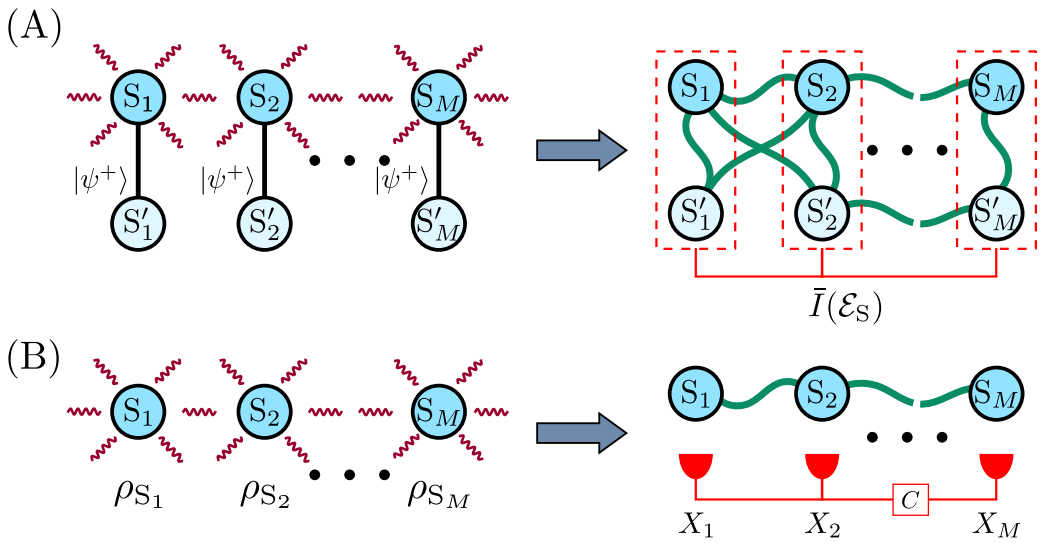

Fig. 8: *Schematic illustration of the multipartite correlation measure. (A) Choi-Jamiołkowski representation of the dynamics. The system is prepared in a product of maximally entangled states of $2M$ parties $\{S_j|S'_j\}$ and the dynamics affects only the subsystems S_j. If and only if the dynamics are correlated, the bipartitions $\{S_iS'_i|S_jS'_j\}$ will be entangled, yielding a nonzero correlation measure $\bar{I}$. (B) Schematic depiction of the procedure to estimate a lower bound of $\bar{I}$. There, the system is initially prepared in a separable state $\rho_{S_1} \otimes \rho_{S_2} \cdots \otimes \rho_{S_M}$ and correlations in the dynamics show up as correlations C (see Eq. (38)) in the measurement of suitably chosen observables $\mathcal{O}_j$. Figure reproduced from [28].*

dynamics can then be assessed by

$$\begin{aligned}\bar{I}(\mathcal{E}_S) &:= \frac{1}{2M\log d} S\left(\rho_S^{CJ} \middle\| \rho_S^{CJ}|_{S_1S'_1} \otimes \ldots \otimes \rho_S^{CJ}|_{S_MS'_M}\right) \\ &:= \frac{1}{2M\log d}\left\{\left[\sum_{i=1}^{M} S\left(\rho_S^{CJ}|_{S_iS'_i}\right)\right] - S\left(\rho_S^{CJ}\right)\right\}, \end{aligned} \tag{36}$$

where $\rho_S^{CJ}|_{S_iS'_i} = \mathrm{Tr}_{\{\forall S_{j\neq i}S'_{j\neq i}\}}(\rho_S^{CJ})$.
A lower bound for the multipartite setting can be applied as shown in Fig. 8(B), by measuring correlations. Mathematically the same steps as in the bipartite case [see Eq. (35)] can be applied, resulting in

$$\bar{I}(\mathcal{E}) \geq \frac{1}{4M\ln d}\frac{C^2_{\rho'}(\mathcal{O}_1,\ldots,\mathcal{O}_M)}{\|\mathcal{O}_1\|^2\ldots\|\mathcal{O}_M\|^2}. \tag{37}$$

Here, $\rho(t)$ is the joint state after the evolution of an initial product state, $\mathcal{O}_1,\ldots,\mathcal{O}_M$ are local observables for the parties $S_1,\ldots,S_M$, respectively, and the correlation function is

$$C_{\rho(t)}(\mathcal{O}_1,\ldots,\mathcal{O}_M) = \langle\mathcal{O}_1\ldots\mathcal{O}_M\rangle_{\rho(t)} - \langle\mathcal{O}_1\rangle_{\rho(t)}\ldots\langle\mathcal{O}_M\rangle_{\rho(t)}. \tag{38}$$

This multipartite bound makes investigating correlation dynamics accessible in systems that are too large for full quantum process tomography, as here the number of measurements increases only linearly compared to the exponential scaling for full quantum process tomography.

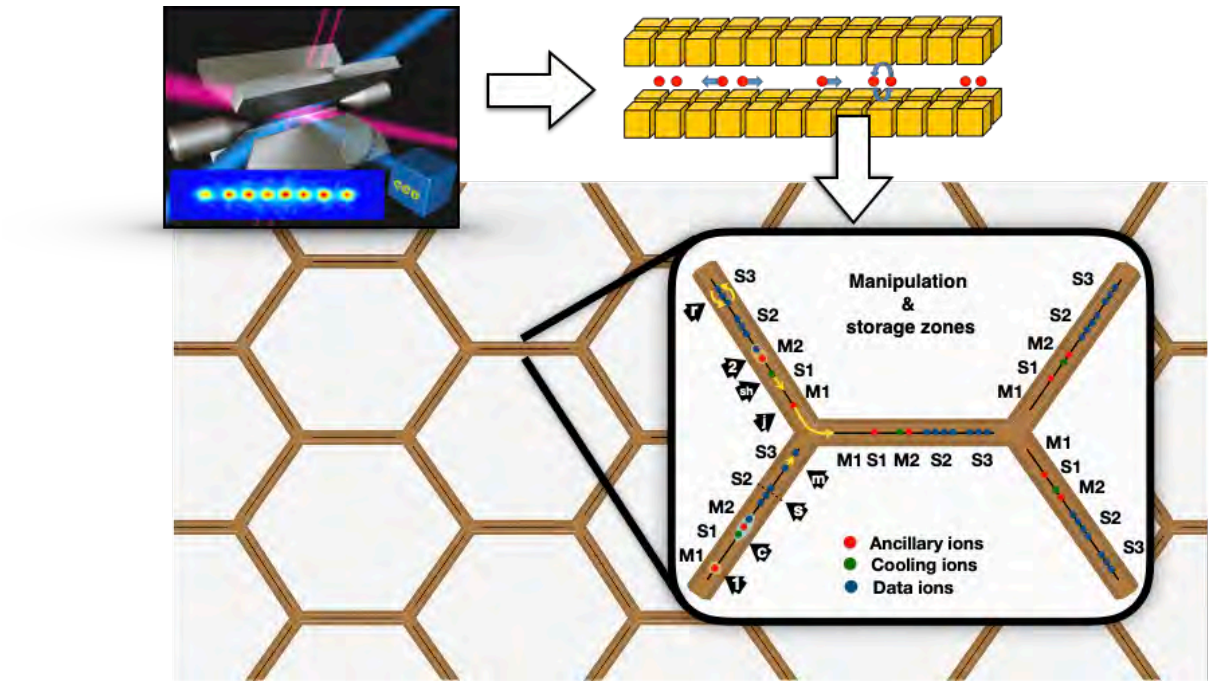

Fig. 9: *Illustration of one scalable route from macroscopic linear Paul traps (upper left) towards large-scale ion-trap quantum processors. Ions can be stored in segmented traps (upper right), where ion crystals can be controlled locally, and ions can be split, moved around and merged with ion-crystals in different trapping regions. This allows one to control increasingly larger qubit registers with high flexibility. Such linear traps can be coupled via junctions, along which ions can be moved from one trap into neighboring zones, where they can be stored (S) or manipulated (M). This will allow one to assemble traps into larger two-dimensional trap arrays, which can be used to host and control large registers of qubits for quantum error correction and eventually large-scale fault-tolerant quantum computation.*

In summary, based on the mapping of quantum dynamics to quantum states in an enlarged Hilbert space via the Choi-Jamiołkowski isomorphism, in this lecture we have discussed a rigorous and systematic method to quantify the amount of spatial correlations in general quantum dynamics. Furthermore, we have applied the theoretical concepts developed to paradigmatic physical models and demonstrated their usefulness for the characterization of noise in experimental quantum processors. We expect that noise characterization techniques such as the ones discussed in this lecture will be of fundamental importance for the study of dynamics in a large variety of quantum systems. From a practical and more applied standpoint, such tools are likely to be essential to make further progress in developing and characterizing increasingly larger and scalable qubits registers, as shown for trapped ions in Fig. 9, to make the dream of large-scale quantum computers and simulators become a reality.

Acknowledgments. I would like to thank my collaborators, Angel Rivas from the Complutense University in Madrid, for the joint theory work of Refs. [25, 28], as well as my colleagues from Rainer Blatt's experimental ion-trapping group at the University of Innsbruck for the joint and joyful collaboration that gave rise to the results of Ref. [28].

References

[1] M. Kjaergaard et al., Annu. Rev. Condens. Matter Phys. **11**, 369 (2020)

[2] C.D. Bruzewicza et al., Appl. Phys. Rev. **6**, 021314 (2019)

[3] H.P. Breuer and F. Petruccione: *The Theory of Open Quantum Systems* (Oxford University Press, 2002)

[4] C.W. Gardiner and P. Zoller: *Quantum Noise* (Springer, Berlin, 2004)

[5] A. Rivas and S.F. Huelga: *Open Quantum Systems. An Introduction* (Springer, Heidelberg, 2011)

[6] R.H. Dicke, Phys. Rev. **93**, 99 (1954)

[7] P. Zanardi and M. Rasetti, Phys. Rev. Lett. **79**, 3306 (1997)

[8] D. Kielpinski, et al., Science **291**, 1013 (2001)

[9] H. Haeffner, et al., Appl. Phys. B **81**, 151 (2005)

[10] T. Monz, et al., Phys. Rev. Lett. **106**, 130506 (2011)

[11] A. Crubellier, et al., J. Phys. B: At. Mol. Phys. **18**, 3811 (1985)

[12] M.A. Nielsen and I.L. Chuang: *Quantum Computation and Quantum Information* (Cambridge University Press, 2010)

[13] D. Aharonov, A. Kitaev and J. Preskill, Phys. Rev. Lett. **96**, 050504 (2006)

[14] J. Preskill, Quant. Inf. Comput. **13**, 181 (2013)

[15] F. Caruso, et al., J. Chem. Phys. **131**, 105106 (2009)

[16] P. Rebentrost, M. Mohseni and A. Aspuru-Guzik, J. Phys. Chem. B. **113**, 9942 (2009)

[17] J. Jeske, J.H. Cole and S.F. Huelga, New J. Phys. **16**, 073039 (2014)

[18] A. Einstein, B. Podolsky and N. Rosen, Phys. Rev. **47**, 777 (1935)

[19] M. Lewenstein, A. Sanpera, and V. Ahufinger: *Ultracold Atoms in Optical Lattices. Simulating quantum many-body systems* (Oxford University Press, 2012)

[20] H.C. Nägerl, et al., Appl. Phys. B **66**, 603 (1998)

[21] M.-D. Choi, Linear Algebra Appl. **10**, 285 (1975)

[22] A. Jamiołkowski, Rep. Math. Phys. **3**, 275 (1972)

[23] M.B. Plenio and S. Virmani, Quant. Inf. Comp. **7**, 1 (2007)

[24] F.G.S.L. Brandão and M.B. Plenio, Nat. Phys. **4**, 873 (2008)

[25] A. Rivas and M. Müller, New J. Phys. **17**, 062001 (2015)

[26] M. Abramowitz and I.A. Stegun: *Handbook of Mathematical Functions* (Dover Publications, New York, 1972)

[27] P. Schindler, et al., New J. Phys. **15**, 123012 (2013)

[28] L. Postler, et al., Quantum **2**, 90 (2018)

[29] T. Ruster, et al., Phys. Rev. X **7**, 031050 (2017)